AIAA JOURNAL
Vol. 41, No. 5, May 2003

Experimental Verification of a Test-Based Hybrid Component Mode Synthesis Approach

Y. Soucy*
Canadian Space Agency, Saint-Hubert, Quebec J3Y 8Y9, Canada
and
J. L. Humar†
Carleton University, Ottawa, Ontario K1S 5B6, Canada

A new approach to component mode synthesis in which the characteristics of individual components are determined experimentally through modal and static tests is described. The component characteristics used in the technique are the mass matrix, rigid-support normal modes and frequencies, residual flexibility attachment modes, and static constraint modes. All component characteristics, except the mass matrix, are obtained through tests. A novelty of the approach is that it allows determination of the test-based characteristics by testing the components when they are attached to supports of arbitrary stiffness. This procedure obviates the need for providing fully rigid or highly flexible supports, as is normally done. In addition, reaction forces at the supports need not be measured during modal testing. The approach has considerable potential for application in testing of large flexible space structures. The theoretical formulation is summarized. The effectiveness of the procedure is experimentally verified by obtaining estimates of the modal parameters of a free–free beam and a free–free grid structure. It is found that the system parameters obtained from the proposed approach exhibit significant improvement in accuracy when a certain minimum number of residual flexibility terms are included in parameter estimation. This is particularly true when the structure being tested is complex.

Nomenclature

a, d, f, k, s	=	vector and matrix subscripts denoting degrees of freedom
$\boldsymbol{F}$	=	external forces imposed during static test
$\boldsymbol{f}$	=	force vector
$\boldsymbol{G}^d$	=	residual flexibility matrix
$\boldsymbol{H}$	=	frequency-response functions (FRFs) in flexible support configuration
$\boldsymbol{H}^*$	=	FRFs in rigid support configuration
$\boldsymbol{I}$	=	identity matrix
$\boldsymbol{K}, \boldsymbol{M}$	=	generalized system stiffness and mass matrices, respectively
$\boldsymbol{k}, \boldsymbol{m}$	=	stiffness and mass matrices, respectively
$\bar{\boldsymbol{k}}, \bar{\boldsymbol{m}}$	=	generalized stiffness and mass matrices, respectively
$\boldsymbol{k}^*$	=	effective constrained coordinate stiffness matrix
$\boldsymbol{p}$	=	generalized Ritz coordinates
$\boldsymbol{q}$	=	independent system generalized coordinates
$\boldsymbol{R}$	=	support reactions produced during static test
$\boldsymbol{T}$	=	transformation matrix from $\boldsymbol{x}$ to $\boldsymbol{p}$
$\boldsymbol{x}$	=	displacement vector
$\boldsymbol{\Gamma}$	=	residual flexibility attachment modes
$\boldsymbol{\Delta}$	=	displacements during static test
$\boldsymbol{\Theta}$	=	diagonal matrix of squared frequencies
$\boldsymbol{\Lambda}$	=	static constraint modes
$\boldsymbol{\Phi}$	=	mass-normalized retained normal mode shapes
$\boldsymbol{\Psi}$	=	submatrix of $\boldsymbol{\Lambda}$ related to displacements along free degrees of freedom
ω	=	frequency of vibration

Received 7 September 2001; revision received 19 December 2002; accepted for publication 20 December 2002.

*Structural Dynamics Engineer, Space Technologies, 6767 route de l'Aéroport.
†Professor, Department of Civil and Environmental Engineering, 1125 Colonel By Drive.

I. Introduction

THE class of methods known as modal synthesis or component mode synthesis (CMS) provides an effective means of dynamic analysis of very large and complex structures. In these methods, the structure is first divided into a number of components. The dynamic characteristics of individual components are usually represented by their normal modes and frequencies, which can be either evaluated from the analysis of the finite element models of the individual components or determined experimentally. These component characteristics are often supplemented by static modes. Models of individual components derived from their dynamic and static characteristics are coupled by using the conditions of compatibility and equilibrium between components at the interfaces. The coupling permits an evaluation of the mode shapes and frequencies of the assembled structure or system, as well as of its response to a specified load.[1]

For large and complex structures, analytical determination of the dynamic characteristics of individual components may be both time consuming and expensive. Also, analytical modeling may involve unacceptable uncertainties. In such situations, the use of modal testing is often the preferred approach for determining the dynamic characteristics.[2] Testing is also useful in validating the finite element models of complex structures. One important application of test-based modal synthesis is in the design and analysis of large space structures. For such structures, testing of the entire assembly is not possible, and component testing provides the only effective alternative.

For test-based CMS methods, the choice of boundary conditions under which modal testing is performed is a key element. Normally, one of two alternative procedures is used in the modal testing of individual components. In one approach, the component is attached to several rigid supports. The attachment points usually include the interface degrees of freedom (DOF). The corresponding fixed-interface normal mode CMS method uses the normal modes and the static constraint modes to characterize the individual component.[3] Although conceptually simple, this approach presents considerable difficulty in practical testing because the construction of truly rigid supports is impractical and expensive. As mentioned by Ewins,[4] approximation of grounded conditions requires extraordinary

precaution in designing the rigid support(s). In the other approach, modal testing of the components is carried out in a free–free configuration. The corresponding free-interface normal mode CMS method uses the normal modes and residual flexibility attachment modes to characterize the individual component.[5] In practice, the test article is suspended by very flexible strings or cables so that the rigid-body mode frequencies are at least an order of magnitude smaller than the fundamental frequency of the test article. A practical difficulty in this method is in providing a truly flexible suspension system. The test procedure usually requires the provision of tall bulkheads for the attachment of cables. In fact, serious problems arise in the testing of zero gravity large space structures. They are so flexible that it is presently quite difficult to design a suspension system with a frequency that is significantly lower than the lowest frequency of the test structure, and even when such a suspension system can be built, it is quite complex and expensive.[6]

Another group of CMS methods comprises methods based on the use of hybrid-interface normal modes for which the component interfaces consist of combinations of free and fixed DOF. Craig and Chang illustrate the use of attachment modes in a hybrid-interface method.[5]

In view of the practical difficulty in providing either truly rigid supports or a suspension system that is very flexible, a new approach to test-based modal synthesis has recently been developed.[7,8] The new procedure is referred to as the experimental hybrid CMS method. The approach allows the determination of fixed-support normal modes and constraint modes from tests on a component attached to supports of arbitrary stiffness. This procedure obviates the need for providing either fully rigid or highly flexible supports. Also, reaction forces need not be measured during modal testing. The suggested procedure, however, relies on an analytical determination of the mass matrix. The experimental hybrid CMS method has considerable potential for application in test-based modal synthesis of large structures, particularly of large and flexible space structures.

The theoretical formulation for the experimental hybrid CMS method has been described in Refs. 7 and 8. Results of computer simulation studies have been presented in Refs. 7 and 9. Those studies have shown that the method is quite feasible and is not very sensitive to the level of errors expected in the estimated component parameters. The focus of the present paper is on the presentation of an experimental verification of the proposed method. For the sake of ready reference, a brief summary of the theoretical formulation is presented in Sec. II. Details of the experimental verification of the procedure based on testing of a free–free beam and a free–free grid structure are given in Secs. III and IV, respectively.

II. Theoretical Background

A. Component Modes

The CMS procedure presented here uses a series of Ritz vectors to represent the motion along the unrestrained physical coordinates of individual components. For the purpose of testing, additional restraints or supports are introduced, thereby fixing several DOF that are unrestrained in the original structure. Such supports are often essential for the testing of very flexible structures, particularly those that are unable to support their own weight under gravity. Some of the additional restrained DOF are in the interior of the component, whereas others are at the interfaces with adjoining components. The first of the series of Ritz vectors is a set of normal modes derived for a configuration in which the component is rigidly supported at all restrained DOF that already exist in the component as well as those that are introduced for the purpose of testing. These rigid-support normal modes $\boldsymbol{\Phi}_{fk}$ are supplemented by constraint modes $\boldsymbol{\Lambda}_{Ms}$ and residual flexibility attachment modes $\boldsymbol{\Gamma}_{fa}$. Because the procedure is based on test data and because a combination of three different types of mode shapes is used, the present method is referred to as the experimental hybrid CMS method.

For a presentation of the theoretical basis consider a system that is divided into two or more free–free components. Each component has several sets of DOF. The total number of DOF in the component is M. These are divided into set s containing DOF that are restrained by supports introduced for the purpose of testing and set f consisting of the free DOF. Set f is further subdivided into subset a of free-interface DOF and subset i of free-interior DOF. There are N_s DOF in set s, N_f DOF in set f, etc.

When damping is neglected, the partitioned equations of motion of a component are expressed as

$$\begin{bmatrix} \boldsymbol{m}_{ff} & \boldsymbol{m}_{fs} \\ \boldsymbol{m}_{sf} & \boldsymbol{m}_{ss} \end{bmatrix} \begin{bmatrix} \ddot{\boldsymbol{x}}_f \\ \ddot{\boldsymbol{x}}_s \end{bmatrix} + \begin{bmatrix} \boldsymbol{k}_{ff} & \boldsymbol{k}_{fs} \\ \boldsymbol{k}_{sf} & \boldsymbol{k}_{ss} \end{bmatrix} \begin{bmatrix} \boldsymbol{x}_f \\ \boldsymbol{x}_s \end{bmatrix} = \begin{bmatrix} \boldsymbol{f}_f \\ \boldsymbol{f}_s \end{bmatrix} \tag{1}$$

where $\ddot{\boldsymbol{x}}$ is the vector of acceleration.

Rigid-Support Normal Modes

These normal modes are obtained from the free-vibration eigenvalue problem derived from the first row partition of Eq. (1), with $\ddot{\boldsymbol{x}}_s$, $\boldsymbol{x}_s$, and $\boldsymbol{f}_f = \boldsymbol{0}$:

$$\left(\boldsymbol{k}_{ff} - \omega^2 \boldsymbol{m}_{ff}\right)\phi = \boldsymbol{0} \tag{2}$$

Solution of Eq. (2) leads to the natural frequencies $\omega_1, \omega_2, \ldots, \omega_{N_f}$ and the corresponding orthonormal mode shapes $\phi_1, \phi_2, \ldots, \phi_{N_f}$. Of the N_f normal modes, only k $(k < N_f)$ modes are retained in the Ritz transformation. The corresponding modal matrix $\boldsymbol{\Phi}_{fk}$ is of dimension $N_f \times k$.

Residual Flexibility Attachment Modes

An attachment mode is a static displacement shape of the component along its free DOF caused by the application in turn of a unit force along each of the free interface DOF, whereas the displacement along the fixed DOF are zero. The attachment modes can be represented by a linear combination of the M rigid-support normal modes and rigid-body modes of the component. Thus, if all M modes were to be included, the attachment modes would be redundant. However, if only some of the normal modes are retained, the contribution of the deleted modes to the displaced shape can be represented by the so-called residual flexibility attachment modes. There exist N_a residual flexibility attachment modes forming the matrix $\boldsymbol{\Gamma}_{fa}$ $(N_f \times N_a)$. These modes are obtained from

$$\boldsymbol{\Gamma}_{fa} = \begin{bmatrix} \boldsymbol{G}^d_{fi} & \boldsymbol{G}^d_{fa} \end{bmatrix} \begin{bmatrix} \boldsymbol{0}_{ia} \\ \boldsymbol{I}_{aa} \end{bmatrix} \tag{3}$$

in which $\boldsymbol{0}_{ia}$ is a null matrix of dimension $N_i \times N_a$, $\boldsymbol{I}_{aa}$ is an identity matrix of dimension N_a, $\boldsymbol{G}^d_{fi}$ and $\boldsymbol{G}^d_{fa}$ are the columns of matrix $\boldsymbol{G}^d_{ff}$ corresponding to the i and a DOF, respectively. Matrix $\boldsymbol{G}^d_{ff}$ is called the residual flexibility matrix. It may be seen as the contribution of the deleted modes to the component flexibility and can be expressed in terms of such modes and the corresponding frequencies as

$$\boldsymbol{G}^d_{ff} = \boldsymbol{\Phi}_{fd} \boldsymbol{\Theta}^{-1}_{dd} \boldsymbol{\Phi}^T_{fd} \tag{4}$$

where $\boldsymbol{\Phi}_{fd}$ are the deleted modes and $\boldsymbol{\Theta}_{dd}$ is the diagonal matrix of squared deleted frequencies. Matrix $\boldsymbol{G}^d_{ff}$ may be obtained either from an analytical model or from results of modal testing.

Constraint Modes

Because the rigid-support normal modes and the residual flexibility attachment modes specify zero displacement along the fixed DOF s, these modes cannot, by themselves, describe a component displaced shape that may include displacements along such fixed DOF. The normal modes and residual flexibility attachment modes are, therefore, supplemented by another set of static displacement shapes, called constraint modes, resulting from the application of a unit displacement in turn at each of the fixed DOF in set s. Constraint modes are given by

$$\boldsymbol{\Lambda}_{Ms} = \begin{bmatrix} \boldsymbol{\Psi}_{fs} \\ \boldsymbol{I}_{ss} \end{bmatrix} \tag{5}$$

where $\boldsymbol{\Psi}_{fs}$, the matrix of static displacements along DOF f, is obtained from

$$\boldsymbol{\Psi}_{fs} = -\boldsymbol{k}^{-1}_{ff} \boldsymbol{k}_{fs} \tag{6}$$

B. Coupling of Components

For each component, the Ritz transformation relating the physical coordinates $\boldsymbol{x}$ to the generalized Ritz coordinates $\boldsymbol{p}$ can be expressed in a partitioned form as

$$\begin{bmatrix} \boldsymbol{x}_f \\ \boldsymbol{x}_s \end{bmatrix} = [\boldsymbol{T}][\boldsymbol{p}] \begin{bmatrix} \boldsymbol{\Phi}_{fk} & \boldsymbol{\Gamma}_{fa} & \boldsymbol{\Psi}_{fs} \\ \boldsymbol{0}_{sk} & \boldsymbol{0}_{sa} & \boldsymbol{I}_{ss} \end{bmatrix} \begin{bmatrix} \boldsymbol{p}_k \\ \boldsymbol{p}_a \\ \boldsymbol{p}_s \end{bmatrix} \tag{7}$$

where $\boldsymbol{T}$ is a transformation matrix. The transformed stiffness and mass matrices may be obtained from

$$\bar{\boldsymbol{k}} = \boldsymbol{T}^T \boldsymbol{k} \boldsymbol{T}, \qquad \bar{\boldsymbol{m}} = \boldsymbol{T}^T \boldsymbol{m} \boldsymbol{T} \tag{8}$$

When $\boldsymbol{T}$ is substituted for and the orthogonality properties of the mode shapes are used, it can be shown that the transformed stiffness matrix in generalized coordinates $\boldsymbol{p}$ is given by

$$\bar{\boldsymbol{k}} = \begin{bmatrix} \boldsymbol{\Theta}_{kk} & \boldsymbol{0} & \boldsymbol{0} \\ \boldsymbol{0} & \boldsymbol{G}^d_{aa} & \boldsymbol{0} \\ \boldsymbol{0} & \boldsymbol{0} & \boldsymbol{k}^*_{ss} \end{bmatrix} \tag{9}$$

where $\boldsymbol{\Theta}_{kk}$ is the diagonal matrix of the squared frequency of the retained normal modes and $\boldsymbol{G}^d_{aa}$ contains the rows of $\boldsymbol{G}^d_{fa}$ corresponding to the a DOF. Matrix $\boldsymbol{k}^*_{ss}$ is a reduced stiffness matrix given by $\boldsymbol{k}^*_{ss} = \boldsymbol{k}_{ss} - \boldsymbol{k}_{sf}\boldsymbol{k}^{-1}_{ff}\boldsymbol{k}_{fs}$; it is referred to here as the effective constrained coordinate stiffness matrix.

The transformed mass matrix is given by

$$\bar{\boldsymbol{m}} = \begin{bmatrix} \boldsymbol{I}_{kk} & \boldsymbol{0}_{ka} & \boldsymbol{\Phi}^T_{fk}(\boldsymbol{m}_{ff}\boldsymbol{\Psi}_{fs} + \boldsymbol{m}_{fs}) \\ \boldsymbol{0}_{ak} & \left(\boldsymbol{G}^d_{fa}\right)^T \boldsymbol{m}_{ff}\boldsymbol{G}^d_{fa} & \left(\boldsymbol{G}^d_{fa}\right)^T(\boldsymbol{m}_{ff}\boldsymbol{\Psi}_{fs} + \boldsymbol{m}_{fs}) \\ \left(\boldsymbol{\Psi}^T_{fs}\boldsymbol{m}_{ff} + \boldsymbol{m}_{sf}\right)\boldsymbol{\Phi}_{fk} & \left(\boldsymbol{\Psi}^T_{fs}\boldsymbol{m}_{ff} + \boldsymbol{m}_{sf}\right)\boldsymbol{G}^T_{fa} & \boldsymbol{\Psi}^T_{fs}\boldsymbol{m}_{ff}\boldsymbol{\Psi}_{fs} + \boldsymbol{\Psi}^T_{fs}\boldsymbol{m}_{fs} \\ & & + \boldsymbol{m}_{sf}\boldsymbol{\Psi}_{fs} + \boldsymbol{m}_{ss} \end{bmatrix} \tag{10}$$

When conditions of compatibility and the standard procedure of direct stiffness assembly are used, the transformed stiffness and mass matrices of individual components are assembled to obtain the global system matrices $\boldsymbol{K}$ and $\boldsymbol{M}$. The mode shapes and frequencies of the assembled structure or system are then obtained by solving the eigenvalue problem

$$\boldsymbol{M}\ddot{\boldsymbol{q}} + \boldsymbol{K}\boldsymbol{q} = \boldsymbol{0} \tag{11}$$

C. Experimental Evaluation of Component Normal and Constraint Modes

To evaluate the transformed stiffness and mass matrices, $\bar{\boldsymbol{k}}$ and $\bar{\boldsymbol{m}}$, we need to know the retained frequencies of the component ω_k, the corresponding mode shapes $\boldsymbol{\Phi}_{fk}$, the residual flexibility submatrix $\boldsymbol{G}^d_{fa}$, the constraint mode submatrix $\boldsymbol{\Psi}_{fs}$, the effective constrained coordinate stiffness matrix $\boldsymbol{k}^*_{ss}$, and the mass matrix. The mass matrix is obtained analytically, whereas the others are obtained through testing.

Normally, the number of measured DOF is much smaller than the number of DOF in the finite element (FE) model. In particular, response along rotational DOF are seldom measured during modal tests due to instrumentation limitation. Consequently, the analytical mass matrix must be reduced to the measured DOF. Mass matrix reduction is part of the larger problem related to the reduction of the property matrices of a system including its analytical mass and stiffness matrices. Issues related to model reduction are as relevant to the testing of a complete system as they are to the testing of a component. They have been dealt with more thoroughly in an extensive body of literature and are outside the scope of present work. It may, however, be stated of the several methods developed for model reduction two of the most popular techniques are the Guyan and system equivalent reduction/expansion process (SEREP) methods. As shown by Avitabile et al.,[10] the Guyan method produces frequencies that are higher than those of the full model, whereas the SEREP method preserves the modal characteristics of the full model for selected modes of interest. Judicious choice of the retained DOF will reduce the possible inaccuracies resulting from reduction of the mass matrix. Such a selection includes deleting the DOF for which the corresponding inertia term is small. Additional work is required on the impact of model reduction and the number and distribution of measured interior DOF on the accuracy of this new experimental CMS approach.

The modal parameters ω_k, $\boldsymbol{\Phi}_{fk}$, and $\boldsymbol{G}^d_{fa}$ are required for a configuration in which the components are fixed along the supported DOF, implying zero displacement along such DOF. As mentioned earlier, provision of truly rigid supports is not a simple task, especially for large complex structures. However, the required parameters can be derived from modal tests on a component whose supports are not fully rigid but have arbitrary stiffness. It can be shown that the frequency response function (FRF) matrix of a component on fully rigid supports, $\boldsymbol{H}^*$, is related to the FRF matrix $\boldsymbol{H}$ for the same structure on supports of arbitrary stiffness by the equation[11]

$$\boldsymbol{H}^*_{ff} = \boldsymbol{H}_{ff} - \boldsymbol{H}_{fs}\boldsymbol{H}^{-1}_{ss}\boldsymbol{H}_{sf} \tag{12}$$

where the matrices of the right-hand side of Eq. (12) are partitions of $\boldsymbol{H}$. The required rigid-support modal parameters are obtained by curve fitting the FRFs that make up $\boldsymbol{H}^*$.

As seen from Eq. (12), excitation locations or driving points must include all supported DOF. Mandatory driving points also include one interior DOF. In practice, at least two interior DOF should be selected as driving point to allow for reciprocity check and to ensure that no modes are missed due to the excitation being located at a modal node. These interior driving points should be well separated to allow for meaningful reciprocity check and should be located where significant deformation is present for the retained modes as predicted by the FE analysis.

Equation (12) contains the inversion of matrix $\boldsymbol{H}_{ss}$, which is related to the supported DOF. Because these supports are introduced only for the purpose of testing, considerable flexibility exists in the selection of their location, subject of course to practical limitations such as local rigidity of the component and ease of attachment. Therefore, the supported DOF may be selected so that they are well separated, which would also be the logical choice to ensure that the component is not damaged under its own weight. With such a selection, individual columns of $\boldsymbol{H}_{ss}$ will be quite distinct, the matrix will be well conditioned, and measurement errors will not cause any problem in obtaining an inverse of the matrix.

The constraint mode submatrix $\boldsymbol{\Psi}_{fs}$ and the effective constrained coordinate stiffness matrix $\boldsymbol{k}^*_{ss}$ are obtained from static tests on the component supported by supports of arbitrary stiffness. As shown in Refs. 7 and 8, $\boldsymbol{\Psi}_{fs}$ is given by

$$\boldsymbol{\Psi}_{fs} = \boldsymbol{\Delta}_{fs}\boldsymbol{\Delta}^{-1}_{ss} \tag{13}$$

where the N_S columns of $\boldsymbol{\Delta}_{ss}$ are linearly independent static displacements imposed along the supported DOF s and $\boldsymbol{\Delta}_{fs}$ contains the corresponding displacements produced along the free DOF f. Also, the effective constrained coordinate stiffness matrix may be expressed as

$$\boldsymbol{k}^*_{ss} = (\boldsymbol{F}_{ss} + \boldsymbol{R}_{ss})\boldsymbol{\Delta}^{-1}_{ss} \tag{14}$$

where $\boldsymbol{F}_{ss}$ are the external forces along the supported DOF that produce displacements $\boldsymbol{\Delta}_{ss}$ and $\boldsymbol{R}_{ss}$ are the corresponding support reactions.

A straightforward procedure is used for obtaining the N_S linearly independent columns of $\boldsymbol{\Delta}_{ss}$. The procedure consists of disconnecting, in turn, each of the supports and imposing a displacement along the DOF released by the removed support. The resulting displacements along the other supported DOF are significantly smaller than the imposed displacement. Consequently, the N_S displaced shapes are linearly independent. Practical details of the procedures are given in Sec. III.

III. Experimental Verification Based on Tests on a Free–Free Beam

The results presented in this paper constitute a part of a test program on experimental verification of the CMS approach and its associated test procedures. The test program included application of the approach to three different systems of increasing complexity. The first system to which the CMS approach was applied was a fixed–fixed beam consisting of two components; the results from that study have been presented in Ref. 12. The results obtained from the application of the CMS method to a free–free beam are given in the present section. Tests on a grid structure are presented in the next section.

A. Flexible Supports

As stated earlier, for the purpose of testing, individual components are supported by supports of arbitrary stiffness. These supports, referred to herein as flexible supports, constitute a key piece of equipment required for the present test program. Such supports are required to create a sufficient number of restrained DOF to prevent large flexible structures, such as spacecraft appendages, from deforming too much and breaking under their own weight. The flexible supports were designed to provide only vertical restraint to the test article at a single location, while allowing freedom of motion in the horizontal plane and about three orthogonal rotation axes. As indicated by Eq. (12), the derivation of even a single column of $\boldsymbol{H}^*$, corresponding to one DOF selected out of f, requires a knowledge of matrices $\boldsymbol{H}_{fs}$ and $\boldsymbol{H}_{ss}$. This implies that an excitation must be applied and the applied excitation, as well as the response, measured along each supported or restrained DOF (set s). Thus, limiting the restrained DOF to only vertical translation significantly reduces the complexity of modal testing [and of static tests to a certain extent, as seen from Eq. (14)].

A flexible support is made up of four separate components: 1) an upper section, 2) two pedestals mounted on the test floor, 3) two upper section fixtures, and 4) an attachment or connection. The upper section consists of a horizontal rectangular bar that provides almost all of the flexibility of the support. The two pedestals rigidly hold the upper section at its extremities, through the upper section fixtures. The attachment is a device that connects the upper section to the test article and is the part that provides the five free DOF. All of the components of a flexible support are visible in Fig. 1, which shows one component of the fixed–fixed beam in a static test configuration.

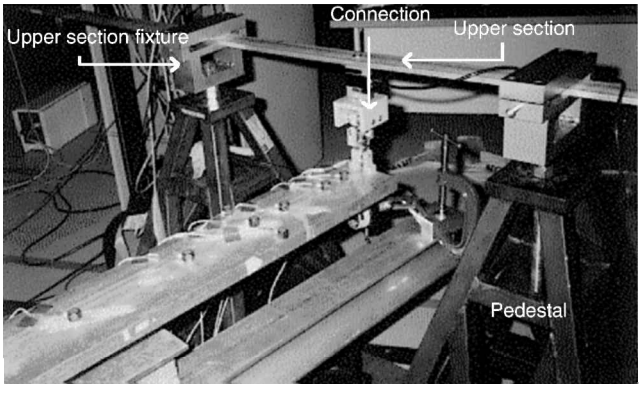

Fig. 1 Flexible support and its components.

B. Test Articles and Boundary Conditions

The free–free aluminum beam to be tested is shown in Fig. 2. It has a length of 9.75 m (32 ft) and a uniform rectangular cross section of 26 × 153 mm. The beam is divided into two components with lengths of 5.18 (17) and 4.57 m (15 ft), respectively. The two components are interconnected at a single node having two DOF, translation in the vertical direction and rotation about an axis perpendicular to the plane of the paper. For the purpose of testing, each component is supported in the vertical direction on three flexible supports at the following locations: at the interface (DOF 1), at 2.44 m (8 ft) from the interface (DOF 9), and at 0.3 m (1 ft) from the other extremity of the component (DOF 17 or 15). For both components, the free interface DOF is labeled 1001.

The rigid-support configuration for component 1 is the target configuration in which there is no displacement along the supported DOF (1, 9, and 17) and with which the $\boldsymbol{H}^*$ related FRFs are associated. The modal parameters obtained by curve fitting the $\boldsymbol{H}^*$ related FRFs are used in the CMS procedure. The test configuration is the one in which the component is attached to flexible supports, located at DOF 1, 9, and 17, and for which the $\boldsymbol{H}$ related FRFs are directly measured.

Because of potential problems in the testing of a 9.75-m-long beam, the reference modal parameters of the free–free beam are obtained through an FE analysis, instead of from modal testing. The modal parameters obtained from test-based CMS will be compared with their reference values. The physical properties (Young's modulus, moment of inertia, mass) used in the analytical models are all based on measurements.

C. Estimation of H^* Through Modal Testing

Test Description and Instrumentation

For the modal test of component 1, that is, the longer beam, a total of 27 accelerometers were fixed on the upper face of the beam (Fig. 3) to measure accelerations in the vertical direction. There were 18 of these accelerometers located on the centerline of the beam along DOF 1–18, at a uniform spacing of 305 mm (1 ft). Six accelerometers were located on either side of the centerline at three different cross sections corresponding to DOF 2, 8, and 16. These sensors were used to identify the torsional modes or coupled

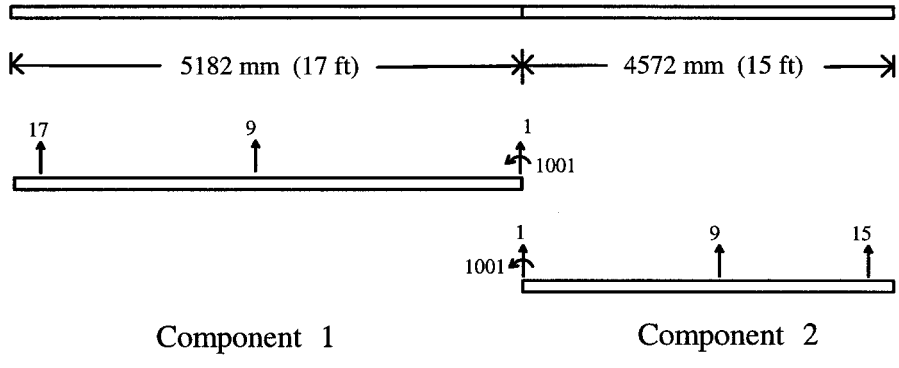

Fig. 2 Free–free beam and its components.

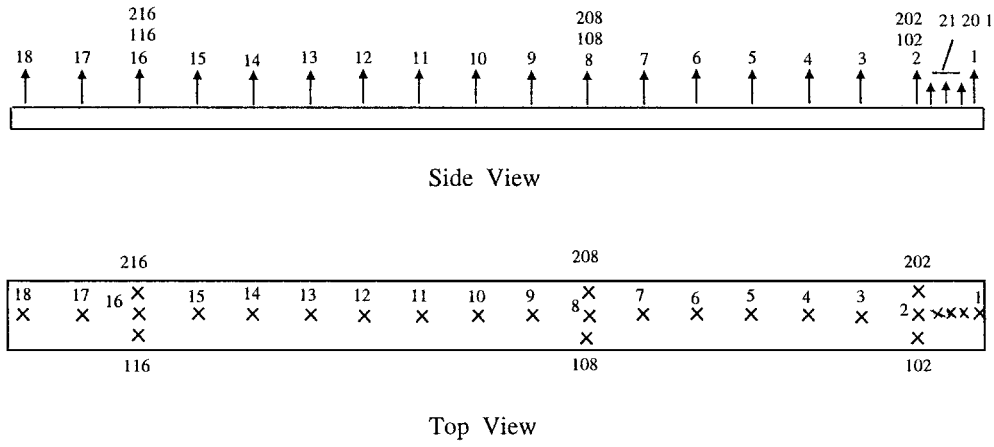

Fig. 3 Location of response DOF for modal testing of component 1 of the free–free beam.

bending and torsional modes of the component. The remaining three accelerometers were located along the centerline of the beam at distances of 50.8 (2 in.), 101.6, and 203.2 mm from DOF 1, corresponding to the DOF 19–21. These three sensors are used in the estimation of rotational FRFs.

The test setup and the instrumentation for component 2 are essentially the same as for component 1. However, because the length of component 2 is smaller than that of component 1 by 610 mm, accelerometers at DOF 18 and 17 do not exist. Also, the two side accelerometers at the cross section corresponding to DOF 16 are instead located on the cross section at DOF 14.

For component 1, excitation was applied at two interior DOF, to allow a reciprocity check to be carried out on the obtained data. These two interior driving points were selected to be at DOF 6 and 11, the latter one being the main interior driving point. Three other driving points were located at the support DOF 1, 9, and 17. In any one test run, simultaneous vertical burst random forces were applied at two different locations. The limit of two excitations was dictated by the capability of the available test hardware. Because the number of excitation locations was greater than two, several runs had to be performed for each component. Each test run was performed with an exciter underneath one of the flexible supports and the other one at the interior driving point of interest. Thus, to obtain one set of $\boldsymbol{H}^*$ related FRFs, three different runs had to be performed.

For component 2, preliminary tests with different driving point locations indicated that a force at DOF 12 best excited all modes of interest; therefore, this DOF was selected as the primary interior driving point. Two other locations, at DOF 2 and 8, were used as driving points for the purpose of the reciprocity check.

For each component, additional driving points were located at DOF 19–21. Test runs were performed with one exciter at one of these three DOF and the other exciter at one of the other interior driving points to obtain estimates of rotational FRFs as explained in a later section. The rotational FRF functions are required to determine the interface rotation element of the mode shapes and for estimation of the residual flexibility terms needed in calculating the residual flexibility attachment modes.

An overview of the test setup is shown in Fig. 4. All components of the flexible supports attached to the test article at DOF 1 and 9 are clearly visible. Also seen are the two exciters located at DOF 11 and 17. The accelerometer cables are visible, although the sensors are not that discernible.

Data acquisition was performed with two different bandwidths: 0–256 and 0–64 Hz. The upper limit of the first bandwidth was high enough to include nine bending modes in the rigid-support configuration. However, the frequency resolution of that bandwidth was too coarse to obtain a good curve fit to the first two modes, due to the very low damping of the test articles. In view of this, the second frequency bandwidth was added, providing a frequency resolution that was four times higher.

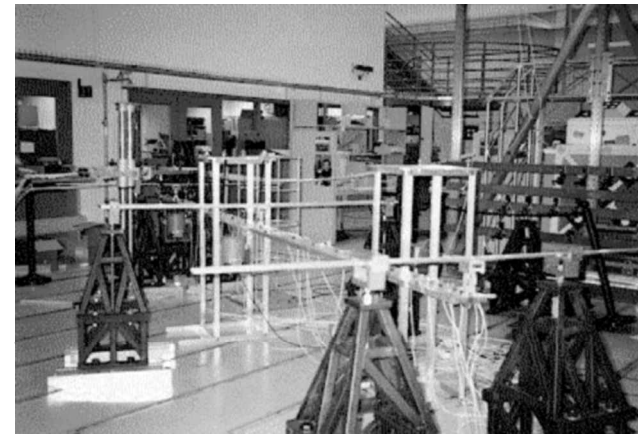

Fig. 4 Overview of modal test setup for component 1 of the free–free beam.

Derived Data in Rigid-Support Configuration

For both components, the results of the reciprocity checks on the translational FRFs at the $\boldsymbol{H}^*$ level, although not shown here, are generally very good to excellent, with all of the peaks corresponding to the bending modes overlapping exactly. This confirms that the test data are consistent and that the flexible supports have a linear behavior.

The $\boldsymbol{H}^*$ related FRF of component 1 for the force and response at DOF 11 is shown in Fig. 5. The first nine bending modes in the frequency bandwidth of interest are identified. Observe that the derived curve is very smooth with all of the modes well defined. The only minor exceptions are the glitches and a fairly low extraneous peak around 30 Hz. The other driving point FRFs of both components were of similar quality.

The interface rotation elements of the mode shapes are obtained by curve fitting the $\boldsymbol{H}^*$ related FRFs involving the response along the rotational DOF. Because measurement of rotational response is still difficult, its value must be derived from the measurements of several translational responses near the point of interest. Sattinger[13] shows that $H_{\theta f}$, in which θ is the rotation at an end of the test article and the force f is at any location, may be approximated by the following forward finite difference expression:

$$H_{\theta_1, f_j} = (-3H_{1j} + 4H_{2j} - H_{3j})/2\Delta \tag{15}$$

where H_{ij} is the FRF relating the translational response at point i to the force at point j and Δ is the distance between two adjacent points i and $i+1$. In the present case, point 1 is at the component interface (DOF 1), whereas points 2 and 3 are 1Δ and 2Δ away from the interface, respectively.

To obtain the residual flexibility attachment modes in the hybrid CMS method, we need the FRFs H_{wm} and $H_{\theta m}$, where w is the

translational displacement at any point, θ is the rotation at an interface DOF, and m is the moment applied at that DOF. Based on Sattinger's[13] work, these two FRFs may be approximated by the following expressions, where Eq. (17) applies to the special case in which the rotation and moment are measured along the same DOF:

$$H_{w_i,m_1} = (-3H_{i1} + 4H_{i2} - H_{i3})/2\Delta \tag{16}$$

$$H_{\theta_1,m_1} = (9H_{11} - 12H_{12} + 3H_{13} - 12H_{21} + 16H_{22} - 4H_{23} + 3H_{31} - 4H_{32} + H_{33})\big/4\Delta^2 \tag{17}$$

Several useful suggestions for deriving rotational FRFs have been proposed by Sestieri et al.[14] In particular, they discuss how an appropriate selection of the spacing between measurement points is crucial in ensuring accuracy of the derived rotational FRFs. The authors mention that a small spacing (with respect to the nodal distance of the highest modes considered) makes the rotational FRFs more precise. However, they add that, the smaller the spacing, the bigger the influence of noise in the data on the finite difference computations.

The rotational FRFs $H^*_{\theta 1,11}$ and $H^*_{\theta 1,m1}$ were derived from the finite difference expressions applied to translational DOF 1, 19, and 20 or 1, 20, and 21. The FRFs were of sufficiently good quality for the estimation of residual flexibility terms.

The translational and rotational $\boldsymbol{H}^*$ related FRFs of component 2 of the free–free beam are of similar quality to that exhibited by the results for component 1.

Estimation of Modal Parameters in Rigid-Support Configuration

For component 1, the modal parameters of the first four bending modes were obtained by curve fitting the $\boldsymbol{H}^*$ related FRFs with respect to the force at DOF 11 and with the frequency bandwidth of 0–64 Hz. Data from all accelerometers, except those at DOF 19–21, were used. The selected rotational FRF was derived from translational measurements at the three points separated by 101.6 mm (DOF 1, 20, and 21). The rotational FRF corresponding to this spacing was selected because the lower spacing of 50.8 mm used later for the higher modes resulted in rotational FRFs that were too noisy. On the other hand, the modal parameters of bending modes 5–9 were obtained by curve fitting the $\boldsymbol{H}^*$ related FRFs with the same excitation point but with a frequency bandwidth of 0–256 Hz. The selected rotational FRF was derived from translational measurements at the three points separated by 50.8 mm (DOF 1, 19, and 20). More details concerning the rotational FRFs are given in Ref. 8.

A comparison of the experimental and analytical frequencies of component 1 in its rigid-support configuration is presented in Table 1. The analytical frequencies are obtained from an FE analysis for a model consisting of 34 beam elements of equal length and with 2 DOF at each node. The physical parameters of the model were obtained experimentally. The differences between the experimental and analytical frequencies are very small, that is, no more than 1% for all nine bending modes. Similar results were obtained for component 2.

The columns of the residual flexibility matrix associated with the free interface DOF, $\boldsymbol{G}^d_{fa}$, are required for computing the transformed component mass matrix as given by Eq. (10). Most advanced commercial software for modal parameter estimation allow extraction of the residual flexibility terms simultaneously with the determination of mode shape residues. However, in the present work, they are estimated separately after determination of the residues using a method described by Bookout[15] and based on work by Rubin.[16]

D. Estimation of Ψ_{fs} and k^*_{ss} Through Static Test

Matrices Ψ_{fs} and $\boldsymbol{k}^*_{ss}$ were derived for each component through static tests in which the component being tested was attached to the same flexible supports as used in the modal tests. The test procedure

Table 1 Comparison between experimental and analytical frequencies, for component 1 of free–free beam in rigid-support configuration

Mode	Experimental frequency, Hz	Analytical frequency, Hz	% Error
1	10.09	10.14	−0.5
2	15.71	15.81	−0.6
3	39.83	40.10	−0.7
4	50.31	50.62	−0.6
5	86.23	87.08	−1.0
6	102.20	102.90	−0.7
7	137.60	139.00	−1.0
8	170.50	171.80	−0.8
9	200.50	202.10	−0.8

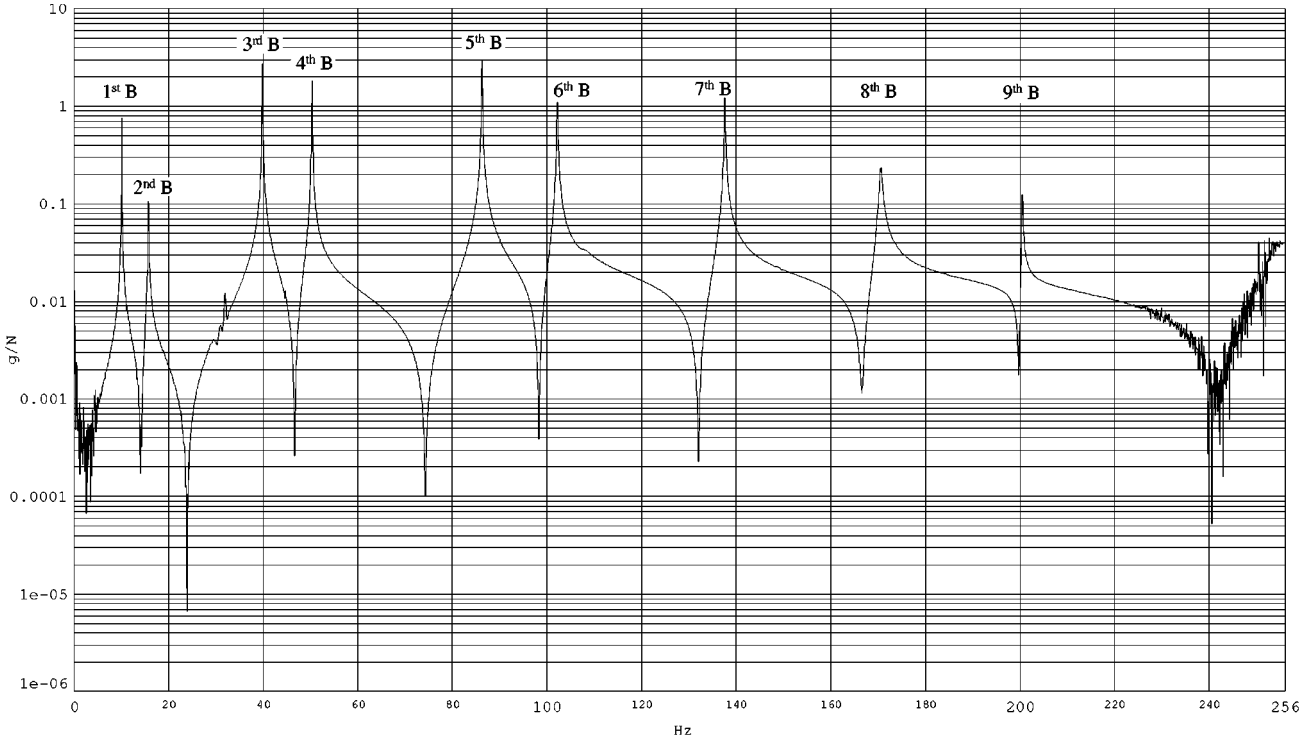

Fig. 5 Drive point H^* FRF at DOF 11 for component 1 of the free–free beam.

consisted of three steps: 1) subject the component to N_S (three for each beam component) linearly independent static displacement shapes along the supported DOF, 2) for each displaced shape, measure the applied force producing the displacements as well as the reaction forces at the supports, and 3) measure the translational displacements at all supported and interior DOF, with the rotation at the interface derived from the measured translational displacements.

The tests were performed by disconnecting, in turn, one of the three flexible supports and applying a series of 9 or 10 different displacements at the location of the removed support. The displacement was applied through a small cable arrangement attached to a S-beam load cell fixed to the test article for measurement of the applied force. For each applied displacement, the corresponding displacements at all supported and free DOF were measured by means of a digital indicator. The corresponding reaction forces at the other two flexible supports were also measured by means of an S-beam load cell.

Measured displacement vs applied load relationships and the reaction force vs applied load relationships were all consistent and linear. The line best fitting the 9- or 10-point data set was estimated through linear regression. The slope of the line gave the displacement (or support reaction) per unit applied force. Rotation at the interface location was estimated through finite difference expressions applied to three equidistant vertical displacements at already instrumented interior DOF, for example, DOF 1, 2, and 3. Measurement along these DOF with a spacing of 305 mm (1 ft), which is larger than that between DOF 1, 19, 20, and 21, is preferred because the static deformed shape of the test article follows a smooth curve with a large radius of curvature.

For this simple structure, the test-based static parameters could be compared with analytical reference values computed by an FE analysis. The agreement between the two was excellent. More specifically, a majority of the test-based static mode shape elements for the translational DOF was in error by no more than 1%. In fact, all translational elements had an error smaller than 2%, except for the element corresponding to DOF 18, which because of its small magnitude had an error of 5.5%. The maximum error in the rotational elements was 5.3%.

The constrained coordinate stiffness matrix $\boldsymbol{k}^*_{ss}$ (size 3×3) was obtained from the measured displacements, applied forces, and reactions using Eq. (14). Note that in the present case $\boldsymbol{R}_{ss}(i, i)$ does not exist because, before application of a force at DOF i, the support at that location is removed. The agreement between $\boldsymbol{k}^*_{ss}$ obtained from measurements and that obtained from an FE analysis was very good, with all nine elements of the $\boldsymbol{k}^*_{ss}$ matrix having an error smaller than 2%.

E. Test-Based CMS Results

When the modal and static component parameters derived from test data as discussed in the preceding paragraphs and the hybrid CMS method were used, estimates were obtained of the system modal parameters. These estimates were compared with the corresponding analytical values. The analytical values were obtained from the analysis of an FE model of the free–free beam system.

The FE models of the free–free beam system and the two components are composed of Bernoulli–Euler beam elements with a length of 305 mm (1 ft). The models are built using consistent mass matrix formulation. The system model has a total of 33 nodes. Components 1 and 2 have 18 and 16 nodes, respectively. Because only in-plane motion is of interest, the initial model of all three structures consisted of two DOF per node. The rotational DOF of these three initial models were condensed out by performing Guyan's reduction. This process resulted in final models for which all DOF correspond to those at which the responses were measured (or derived from measurements as in the case of interface rotations) during component tests. Each node of the final system model has one DOF, vertical translation. For each of the final component models, the node located at the interface has two DOF: vertical translation and in-plane rotation; the interior points have only one DOF, vertical translation. The physical and elastic properties, that is, the width and thickness of the cross section, the material density, and Young's modulus, required in the generation of the FE models were obtained through measurement, as detailed in Ref. 8.

For a comparison of the two sets of modal parameters, two different error measures are defined. The percentage error in frequencies is given by

$$e_\omega = (\omega_a - \omega_r)/\omega_r \times 100 \tag{18}$$

where ω_a is the frequency approximation obtained from the CMS and ω_r is the reference or "exact" frequency obtained from finite element analysis.

The error measure for the mode shapes is defined as

$$e_\varphi = \left[\frac{(\varphi_a - \varphi_r)^T (\varphi_a - \varphi_r)}{\varphi_r^T \varphi_r} \right]^{\frac{1}{2}} \times 100 \tag{19}$$

where φ_a is the mode shape approximation and φ_r is the reference mode shape.

Errors in the estimated test-based system frequencies are shown in Fig. 6a for two cases of different numbers of retained component normal modes. The CMS frequencies are obtained by completely ignoring the residual flexibility terms. When nine and eight modes are retained for components 1 and 2, respectively, the system frequency error for the first mode is 4.0%. This is a reasonable value considering that it is obtained by neglecting the residual flexibility effects and that the error in computer simulation for the same case is 2.7%. Note that simulation errors are computed by comparing the values of modal parameters obtained from the analysis of an FE model of the complete beam and those obtained from separate analyses of the two components followed by a component mode synthesis. For test-based modes 2–9, the frequency errors are quite small, being no more than 2%.

When only $4 + 3$ modes are retained, the frequency errors are somewhat higher than in the earlier case, as would be expected. The error in the first mode of the system is 6.6%. Although not negligible, this value should be viewed in light of the fact that the simulation error for the same condition is 5.2%. The frequency errors for modes 2 and 4 are very small, being less than 1%. The error for mode 6 is also small, less than 2%. The errors for modes 3, 5, and 7 are also fairly small, less than 5%. Errors in frequency for modes 8 and 9 are still acceptable, being no more than 7% despite that a total of only seven normal modes are retained at the component level.

The third curve in Fig. 6a, labeled $4 + 3$ ($w\,\boldsymbol{G}_{aa}$), corresponds to the case when the test-derived interface residual flexibility term $\boldsymbol{G}^d_{aa}$ is accounted for but all other residual flexibility terms, $\boldsymbol{G}^d_{ia}$, are neglected. The error in the first system frequency is reduced from 6.6 to 2.2%. The error for the third mode is reduced to less than 1%.

The errors in the estimated system mode shapes are shown in Fig. 6b. As expected, they tend to increase with the order of the system modes and with a smaller number for the retained normal modes. For the case of $9 + 8$ retained modes, the errors are fairly small, being no more than about 10% in the first nine modes. When only $4 + 3$ modes are kept, the errors become larger but are still acceptable for the lower system modes, being no more than 10% for the first four modes. These errors are very similar to the corresponding simulation values. Evidently the large errors in the higher modes arise because the number of retained modes is small.

Observe from Fig. 6b that, when the interface residual flexibility term is included, significant reduction in the errors for system modes occurs. When $4 + 3$ modes are retained and residual flexibility is taken into account, the error is no more than 4% in the first four modes. On the basis of these results, and others not presented here, it could be suggested that, provided the residual flexibility is accounted for, the number of retained modes in each component should be about the same as the total number of system modes being sought.

IV. Experimental Verification Based on Tests on a Free–Free Grid

The tests on the free–free grid structure are described in the present section. Obviously, the grid structure is more complex than the free–free beam. This increased complexity arises from 1) the

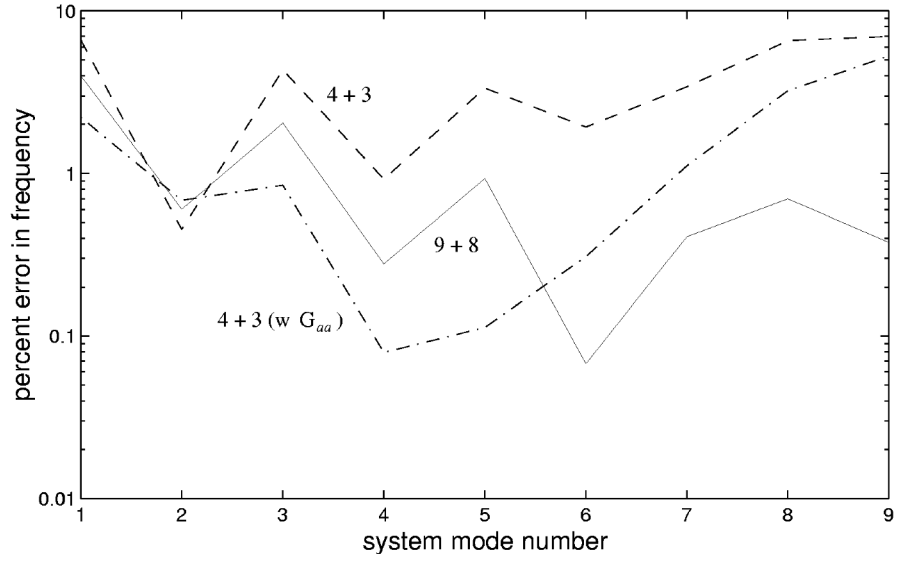

Fig. 6a Errors in frequencies of the free–free beam obtained from CMS with test-based component parameters.

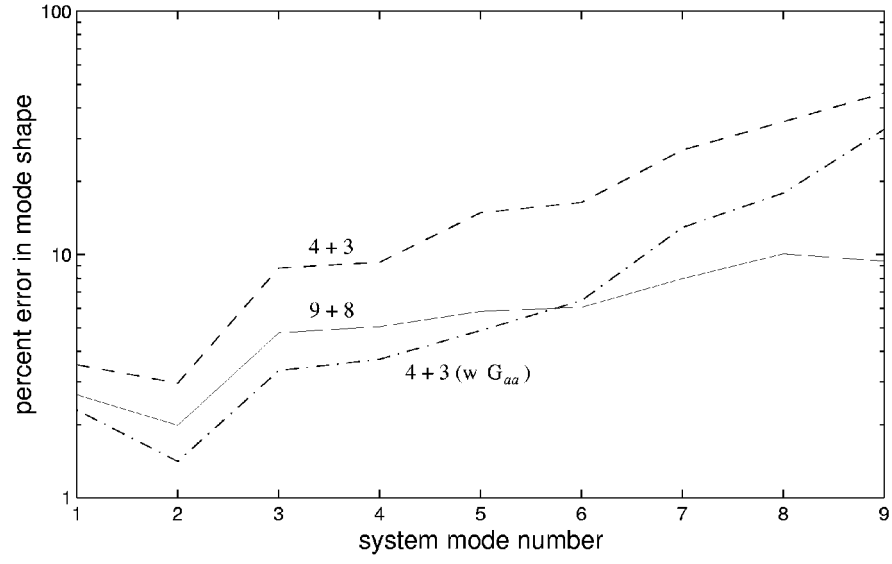

Fig. 6b Errors in mode shapes of free–free beam obtained from CMS with test-based component parameters.

greater number of flexible supports to which the component test articles are attached, four instead of three for the beam components; 2) the greater number of free interface DOF, four instead of one; and 3) the greater uncertainty in obtaining analytical values for the mass and stiffness matrices. Because the test of the free–free grid is concerned only with the out-of-plane motion, in-plane displacements and rotations are not included as interface DOF and are not measured.

A. Test Articles and Boundary Conditions

The grid is designed as a flat structure with 2 main longerons, 10 cross members at right angle, and 8 diagonals, as shown in Fig. 7. The overall length of the grid is 5432 mm. The spacing of the longerons is 1023 mm between outer edges. The grid is produced by assembling two components of lengths 2751 and 2681 mm, respectively, as identified in Fig. 7. The numbers, from 1 to 58, in Fig. 7 denote the nodes of the system FE model. This analytical model was developed to obtain the required mass matrices for CMS and the reference modal parameters to which the test-based CMS results are compared. All elements of the grid system are made of aluminum. The longerons are made of T sections with dimensions $38.10 \times 38.10 \times 4.8$ mm. The stem of the T lies in the plane of the grid. The cross members and diagonals are made of solid rectangular bars with dimensions of 12.7×25.4 mm, the smaller dimension being in the plane of the grid. Connections between the longerons, cross members, and diagonals are made through an aluminum solid block to which the individual members are welded.

The grid represents part of a stiffening support structure that could form the backbone of a radar array appendage of a satellite. It was built for the Canadian Department of National Defense and transferred to the Canadian Space Agency for use in its ongoing research and development projects.

For the purpose of testing, each component of the grid was supported by four flexible supports attached to the solid blocks of the components, at the two blocks located at component interfaces (nodes 28 and 31 in Fig. 7) and at two other blocks located one bay before the opposite end of the component, that is, at nodes 8 and 10 for component 1 and at nodes 49 and 51 for component 2.

B. Estimation of H^* Through Modal Testing

Test Description and Instrumentation

The test setup, instrumentation and data acquisition procedures were exactly the same for both components. Figure 8 shows component 1. The numbers in Fig. 8 indicate the locations of the translational DOF used for response measurements. Locations 1 and 2 represent the two nodes constituting the interface. The interface consists of six DOF: four free rotational DOF (two at each node), and two vertical fixed DOF.

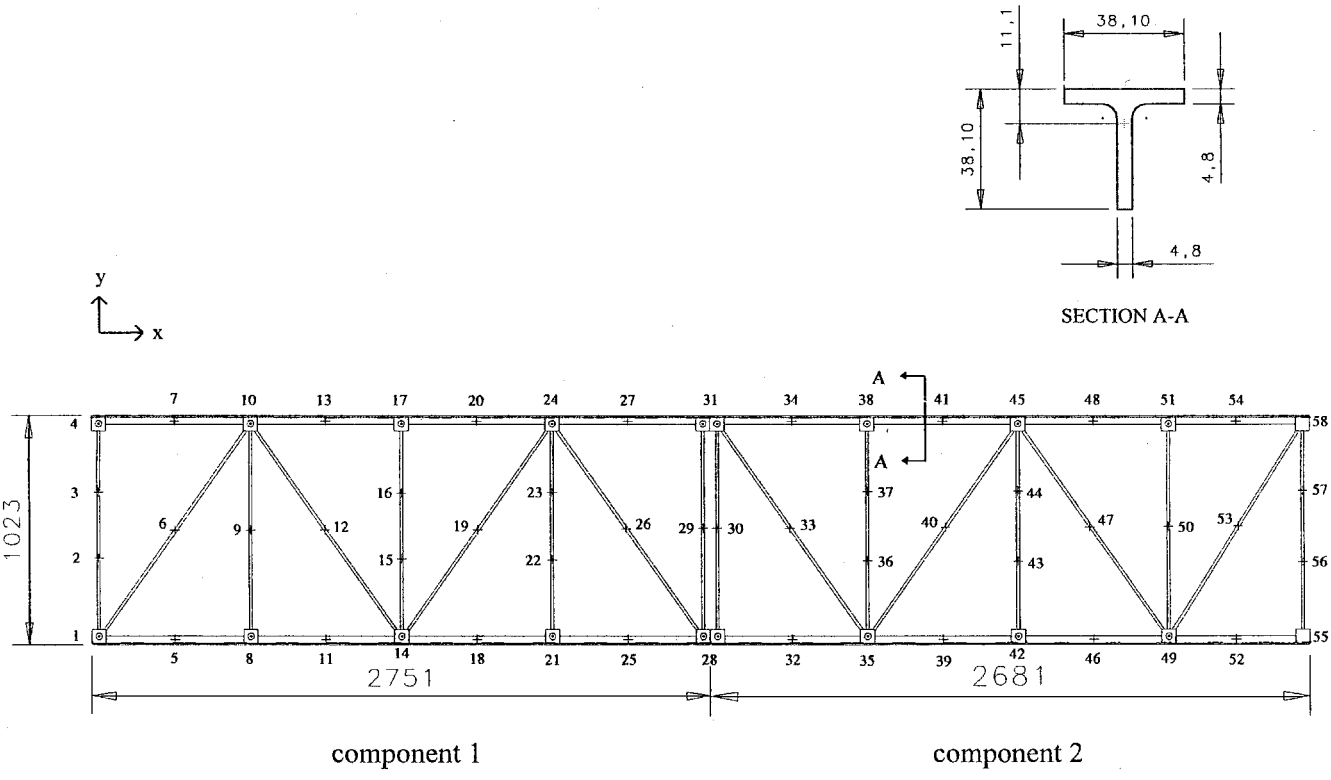

Fig. 7 Grid structure showing the finite element node numbers; all dimensions in millimeters.

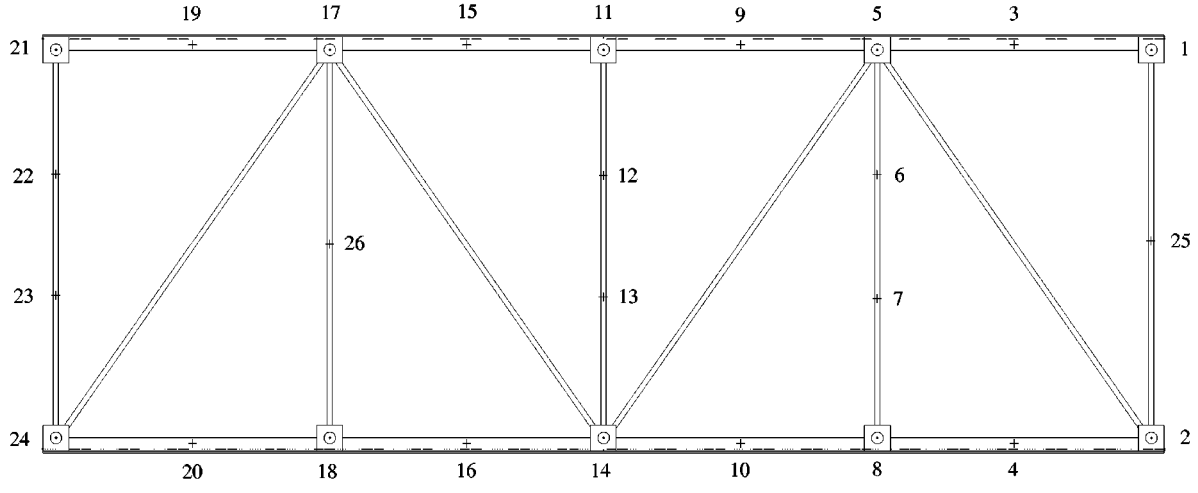

Fig. 8 Location and numbering of DOF for both components of the grid structure.

For the modal tests, one accelerometer was fixed vertically on the upper surface of the grid at each of the 26 locations shown in Fig. 8 on the longerons, the cross members, and the solid blocks, including those at the supported DOF. Rotational FRFs at the two interface locations (DOF 1 and 2) were obtained from translational FRFs using the method of simple difference and measurements at two locations on a solid block, which could be considered as being essentially rigid. To this end, two accelerometers were added on the upper face of each of the two solid blocks, the corresponding locations denoted as 101 and 201 on block at node 1 and 102 and 202 on block at node 2.

Two locations were selected for the main interior driving points, namely, DOF 4 and 15. Between them, the two driving points sufficiently excite each mode of interest. The four supported DOF constituted additional driving points, as required for the derivation of the $\boldsymbol{H}^*$ related FRFs. Also, excitation had to be applied at DOF 101, 102, 201, and 202 to derive the FRFs corresponding to the four interface moments.

Data acquisition with a single frequency bandwidth of 0–128 Hz was sufficient to obtain the first 15 global modes of the component in the rigid-support configuration. The requirement related to the application of excitation at the 10 driving points identified in the preceding paragraph meant that a total of 5 runs had to be carried out, each with 2 exciters at different locations. Figure 9 shows an overview of the test setup with the exciters located at DOF 2 and 15.

Derived Data in Rigid-Support Configuration

A reciprocity check between DOF 4 and 15 for component 1 showed excellent match, with all of the peaks corresponding to at least the first 9 bending modes overlapping exactly and any differences in modes 10 to 15 being quite small. Similar results were obtained for component 2.

The $\boldsymbol{H}^*$ related FRF of component 1 for the force and response at DOF 4 is shown in Fig. 10. There are 14 of the first 15 global modes of the component identified with the corresponding peaks. The curves are very smooth with only a few small glitches and

extraneous peaks. Some of these anomalies may correspond to local modes corresponding to in-plane vibration of diagonals and cross members. However, such in-plane modes are not easily identified from the present data because all response measurements are made in the out-of-plane direction only.

As already mentioned, rotational FRFs were derived using the method of simple difference based on data from two adjacent accelerometers on a single interface block. The eight rotational $\boldsymbol{H}^*$ related FRFs, corresponding to the four interface rotations and the two driving points, were derived for each component. The matrix of residual flexibility associated with the interface DOF, $\boldsymbol{G}_{aa}^d$, has dimensions 4 by 4. There are 16 $\boldsymbol{H}^*$ related FRFs, each with an interface rotation as response and an interface moment as input, required to determine $\boldsymbol{G}_{aa}^d$. These FRFs were also obtained from the translational measurements using the method of simple difference. In fact, as discussed later, only the diagonal coefficients of $\boldsymbol{G}_{aa}^d$ that correspond to the drive point rotational FRFs, are used in the present work.

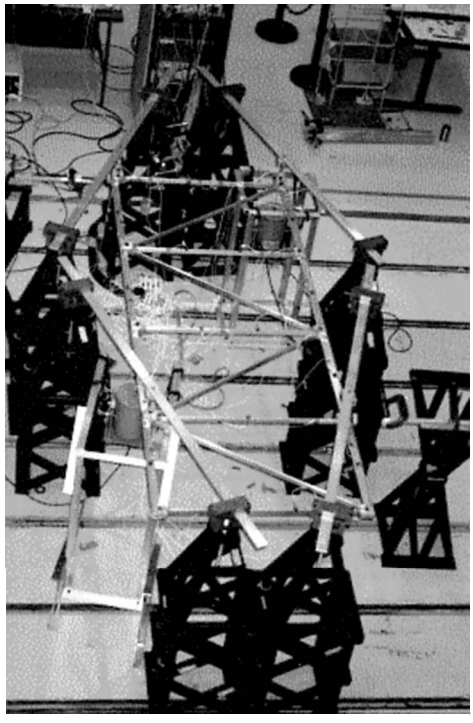

Fig. 9 Overview of modal test setup for a grid component.

Estimation of Modal Parameters in Rigid-Support Configuration

For both components, the poles (containing frequency and damping values) corresponding to the first 15 modes were obtained by curve fitting simultaneously the 44 $\boldsymbol{H}^*$ related FRFs associated with the response at the interior DOF and the force at DOF 4 and 15. The eight rotational FRFs were added for mode shape estimation.

A comparison between the experimental and analytical frequencies of component 2 is presented in Table 2. The analytical values are obtained from the full FE model of component 2. This model consists of 6 DOF at each of the nodes shown in Fig. 7. Except for the case of second mode, which shows an error of 6.3%, all other errors are less than 5%, most of them being less than 2.5%. The modes with the highest error (modes 2, 4, and 6) consist mainly of

Table 2 Comparison between experimental and analytical frequencies for component 2 of free–free grid in rigid-support configuration

Mode	Experimental frequency, Hz	Analytical frequency, Hz	% Error
1	7.78	7.61	2.2
2	16.84	15.84	6.3
3	18.53	18.10	2.4
4	29.31	28.04	4.5
5	40.09	39.15	2.4
6	51.40	49.40	4.0
7	63.27	63.24	0.0
8	64.79	64.99	−0.3
9	75.31	74.75	0.7
10	86.90	85.07	2.2
11	91.41	91.36	0.1
12	94.97	93.54	1.5
13	100.50	97.10	3.5
14	101.30	98.48	2.9
15	105.40	101.90	3.4

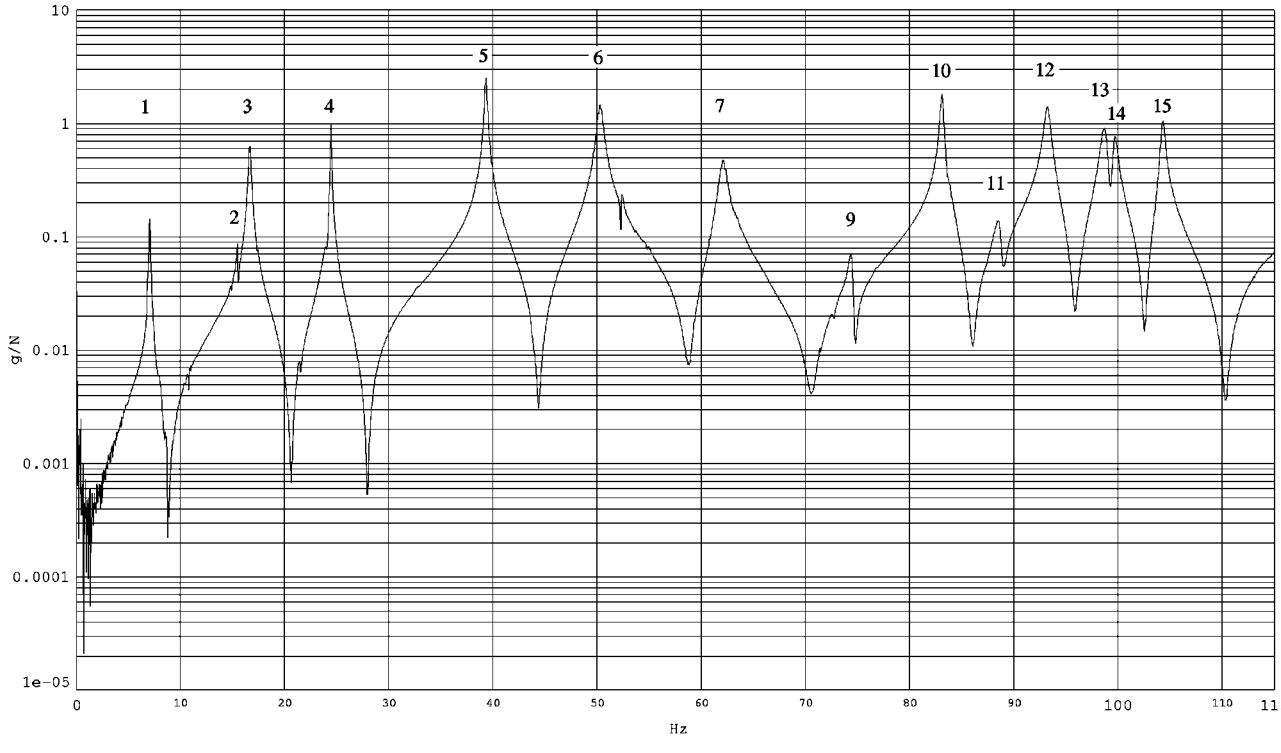

Fig. 10 Drive point H^* related FRF at DOF 4 for component 1 of the grid structure.

overall torsion of the component. A similar comparison for component 1 shows slightly better results. When the relative complexity of the test articles and that no model updating has been done based on test data are considered, the agreement between the experimental and analytical frequencies is quite good.

C. Estimation of Ψ_{fs} and k^*_{ss} Through Static Test

The procedure used for obtaining Ψ_{fs} and k^*_{ss} through static tests was similar to that used for the free–free beam. For derivation of rotation at the interface, an extension aluminum bar with rectangular cross section was fixed in succession in two orthogonal directions at each of DOF 1 and 2. Vertical displacements were measured at three equidistant points on the bar separated by 279 mm. Several estimates of rotations were then made using simple difference and finite difference expressions.

The estimated test-based static parameters were compared with their reference values computed from an FE model. The match between the two sets of values was very good.

D. Test-Based CMS Results

The hybrid CMS method was implemented using the modal and static component parameters derived from test data as described in the preceding paragraphs. The estimated approximate system modal parameters are compared here with the corresponding reference parameters. The reference parameters are obtained from the analysis of an FE model of the grid structure. This model consists of beam elements and lumped mass elements representing the rigid blocks. The full model consists of 58 nodes having 6 DOF at each node. By the use of static condensation and Guyan's reduction, the model is reduced to 50 active nodes with one DOF per node (out-of-plane translation). These active DOF correspond to the locations and direction of the response measurements made during the tests.

The errors in the estimated system frequencies are shown in Fig. 11a for two cases of different numbers of retained component normal modes. The CMS frequencies are first obtained by completely ignoring the residual flexibility terms. When 15 modes are retained for each component, the errors in system frequencies for all of the modes, except the first one, are reasonably small, being no more than 6.5% as seen in the curve labeled 15 + 15. The error for the first mode looks a bit large at 11.2%. However, when it is considered that the residual flexibility has been completely neglected and that the error in the corresponding simulation value, not shown here, is 6.6%, the test-based results may be considered acceptable. When only 6 + 6 modes are retained, the frequency errors become quite high, with only two of the nine modes having an error less than 10% and five modes having an error higher than 20%. However, except for the first mode, the levels of error are fairly similar to the corresponding values obtained from a simulation.

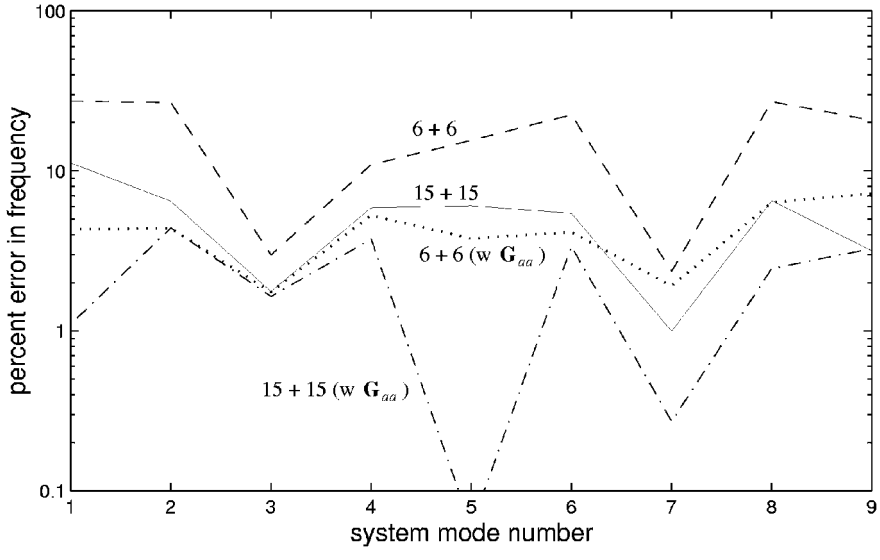

Fig. 11a Errors in frequencies of the grid system structure obtained from CMS with test-based component parameters.

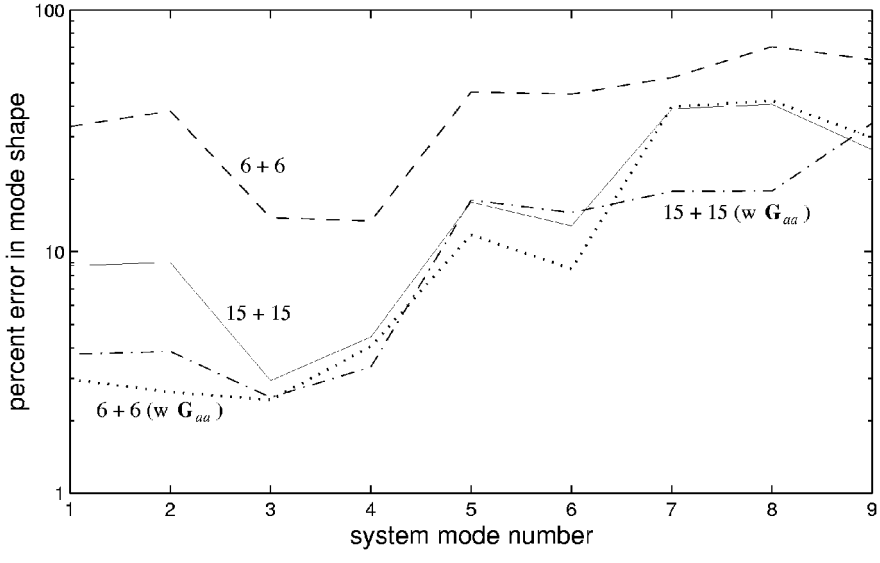

Fig. 11b Errors in mode shapes of the grid structure obtained from CMS with test-based component parameters.

The two curves of Fig. 11a identified with the additional $w\,\boldsymbol{G}_{aa}$ represent the case for which the residual terms of $\boldsymbol{G}^d_{aa}$ are accounted for. In fact, only the diagonal terms (drive points) of the two 4×4 matrices are used. From the curve labeled $15 + 15$ ($w\,\boldsymbol{G}_{aa}$), it is seen that the frequency error for the first mode has been reduced from 11.2 to 1.1%. The errors for modes 1, 3, 5, and 7, which correspond to the first four bending modes of the system, are all less than 2%. The frequency errors for modes 2, 4, 6, and 8, which are mainly torsion modes, vary between 2.5 and 4.4%. For the case when only $6 + 6$ modes are retained but the four residual terms are included, a significant drop in errors is observed when compared to the case for which the $6 + 6$ modes are used without residual flexibility. The errors for six of the first nine modes are seen to be less than 5%, and errors for the other three modes are less than 7.5%.

The errors in the estimated system mode shapes obtained from test-based CMS are shown in Fig. 11b. When $15 + 15$ modes are retained, the errors in the first 4 modes for both cases, those with and without residual flexibilities, are quite small. In fact, six of the eight values have an error of less than 5%, whereas the other two have errors below 9%. The errors for modes 5 and 6 are also acceptable, lying between 13 and 18%. The error for modes 7 and 8 for the case without residuals is quite large, being about 40%. However, the error is not much larger than the corresponding simulation values, which is about 33%. The mode shape errors for mode 9 are also quite large, at 26 and 34%. However, these errors are lower than the corresponding simulation value, which is 39%. For four modes, inclusion of residual flexibility terms leads to a significant reduction in the errors.

From Fig. 11b, it is seen that, for the case when $6 + 6$ modes are kept without accounting for residual flexibility, the shape errors are quite large for all modes, except for modes 3 and 4, for which the errors are acceptable at about 13%. Computer simulation shows errors of similar magnitudes. Evidently, these large errors arise, at least partly, because the number of retained modes is small. When the estimated residual terms are taken into account, the errors drop significantly for all modes.

Note that only 4 of the 16 coefficients of $\boldsymbol{G}^d_{aa}$ are sufficient to obtain considerable reduction in the errors. The off-diagonal terms could also be added. However, such addition does not result in any significant improvement. Besides, experimental determination of reasonably accurate values of the off-diagonal terms is quite difficult because they are associated with the transfer FRFs that is, different DOF for input and response, as opposed to drive point FRFs.

V. Summary

A new test-based method developed by the authors for estimating the frequencies and mode shapes of a large structure by synthesizing the characteristics of its components is described. The component characteristics used in the method consist of rigid-support normal modes, residual-flexibility attachment modes, and constraint modes. These characteristics are derived from modal and static tests on the components, which are held by supports of arbitrary stiffness. This procedure eliminates the need for providing either very flexible supports or completely rigid supports, both of which pose considerable practical difficulty, especially for large flexible space structures.

Results obtained from tests on two components of a free–free beam and a free–free grid structure are presented to demonstrate the effectiveness of the method. The errors in the frequencies of the free–free beam obtained by the test-based component mode synthesis are no more than 4% for the first nine modes when eight and nine component normal modes are retained and all residual flexibility terms are neglected. For the more complex grid system, the frequency errors for the first 9 modes are less than 5% when 15 normal modes are retained for each component and only part of the residual flexibility terms are accounted for.

The test results confirm the prediction based on simulation that the inclusion of residual flexibility terms always reduces the errors in the derived system parameters. The level of improvement depends on the characteristics of the structure being tested. Note that, when the residual flexibility terms are included, the test-based hybrid CMS method provides reasonably accurate estimates of the lowest frequencies and mode shapes, equal in number to the minimum number of measured component frequencies and mode shapes.

In summary, the test results reported here confirm the validity and effectiveness of the proposed test-based hybrid CMS method in obtaining the vibration characteristics of a system. The main application of the method is to systems that are large in size, so that the modal testing of the complete system is impractical. In fact, it is well known that, for large systems that are assembled from components manufactured at different sites, the CMS presents a special advantage. Obviously, the success of the procedure depends on how accurately the component frequencies and mode shapes can be measured. Modal testing of complex systems presents many challenges, but this is as true of measurements at the system level as it is at the component level.

References

[1]Craig, R. R., Jr., "A Review of Time-Domain and Frequency-Domain Component-Mode Synthesis Methods," *International Journal of Analytical and Experimental Modal Analysis*, Vol. 2, No. 2, 1987, pp. 59–72.

[2]Baker, M., "Component Mode Synthesis Methods for Test-Based Rigidly Connected Flexible Components," *Journal of Spacecraft and Rockets*, Vol. 23, No. 3, 1986, pp. 316–322.

[3]Craig, R. R., Jr., and Bampton, M. C. C., "Coupling of Substructures for Dynamics Analysis," *AIAA Journal*, Vol. 6, 1968, pp. 1313–1319.

[4]Ewins, D. J., *Modal Testing: Theory and Practice*, Research Studies Press, Letchworth, England, U.K., 1984, pp. 90, 91.

[5]Craig, R. R., Jr., and Chang, C.-J., "On the Use of Attachment Modes in Substructure Coupling for Dynamic Analysis," *Proceedings of the AIAA/ASME 18th Structures, Structural Dynamics, and Materials Conference*, Vol. B, AIAA, New York, 1977, pp. 89–99.

[6]Cooley, V. M., and Giunta, A. A., "Laboratory Evaluation of Two Advanced Suspension Devices for Ground Vibration Testing of Large Space Structures," *Proceedings of the AIAA/ASME/ASCE/AHS/ASC 33rd Structures, Structural Dynamics, and Materials Conference*, Pt. 3, AIAA, Washington, DC, 1992, pp. 1700–1710.

[7]Humar, J. L., and Soucy, Y., "Hybrid Component Mode Synthesis," *Computers and Structures*, Vol. 67, 1998, pp. 503–515.

[8]Soucy, Y., "Test-Based Hybrid Component Mode Synthesis," Ph.D. Dissertation, Dept. of Civil and Environmental Engineering, Carleton Univ., Ottawa, 1998.

[9]Soucy, Y., and Humar, J. L., "Computer Simulation of Test Based Modal Synthesis," *Proceedings of the CSCE Third Canadian Conference on Computing in Civil and Building Engineering*, Canadian Society for Civil Engineering, Montreal, 1996, pp. 432–443.

[10]Avitabile, P., O'Callahan, J., and Milani, J., "Comparison of System Characteristics Using Various Model Reduction Techniques," *Proceedings of the 7th International Modal Analysis Conference*, Society for Experimental Mechanics, Bethel, CT, 1989, pp. 1109–1115.

[11]Salvini, P., and Sestieri, A., "Predicting the Frequency Response Function of a Structure When Adding Constraints," *International Journal of Analytical and Experimental Modal Analysis*, Vol. 8, No. 1, 1993, pp. 55–62.

[12]Soucy, Y., and Humar, J. L., "Experimental Verification of a New Test Based Modal Synthesis Approach," *Proceedings of the 16th International Modal Analysis Conference*, Society for Experimental Mechanics, Bethel, CT, 1998, pp. 1125–1131.

[13]Sattinger, S. S., "A Method for Experimentally Determining Rotational Mobilities of Structures," *Shock and Vibration Bulletin*, Vol. 50, Pt. 2, 1980, pp. 17–27.

[14]Sestieri, A., Salvini, P., and D'Ambrogio, W., "Reducing Scatter from Derived Rotational Data to Determine the Frequency Response Function of Connected Structures," *Mechanical Systems and Signal Processing*, Vol. 5, No. 1, 1991, pp. 25–44.

[15]Bookout, P. S., "Statistically Generated Weighted Curve Fit of Residual Functions for Modal Analysis of Structures," NASA TM 108481, Feb. 1995, pp. 8–16.

[16]Rubin, S., "Improved Component-Mode Representation for Structural Dynamic Analysis," *AIAA Journal*, Vol. 13, No. 8, 1975, pp. 995–1006.

C. Pierre
Associate Editor